COMPOSITIONAL VARIATION OF ARSENOPYRITE AND FLUID EVOLUTION AT THE ULSAN DEPOSIT, SOUTHEASTERN KOREA: A LOW-SULFIDATION PORPHYRY SYSTEM

SEON-GYU CHOI[§] AND SEUNG-JUN YOUM

Department of Earth and Environmental Sciences, College of Science, Korea University, 1, Anam-dong, Seongbuk-ku, Seoul 136-701, Korea

ABSTRACT

The Ulsan Fe–W mine is located within the Cretaceous Gyeongsang volcano-sedimentary basin at the southeastern edge of the Korean Peninsula. Distinct hydrothermal events resulted in calcic skarn and vein deposits in recrystallized limestone near a Tertiary epizonal granite stock. The deposits of the Ulsan mine present a unique opportunity to document geochemically the complex evolution of a skarn–vein system that is related genetically to a low-sulfidation system. Isochemical contact metamorphism of an early skarn stage (stage I) is displayed by the presence of anhydrous Ca–Al–Mg skarn minerals at the contact between granite and recrystallized limestone. Following magnetite deposition in the main prograde skarn (stage II), the first deposition of arsenopyrite occurs intergrown with rammelsbergite – niccolite – gersdorffite – löllingite – native bismuth – bismuthinite – hexagonal pyrrhotite. These common sulfide assemblages are characterized by an overall low-sulfidation state during the main skarn stage. Retrograde skarn (stage III) is characterized by minor impregnations of scheelite in calcite and quartz, with actinolite and chlorite. During the latest part of stage III, Cu–Zn and polymetallic sulfide mineralization was introduced. The latest episode in the hydrothermal system (stage IV) is characterized by Zn–Pb–Ag mineralization in siderite–quartz veins. Decreasing As contents in arsenopyrite from stages II to IV indicate a decrease in temperature or sulfur fugacity (or both) with time. The various skarn-forming events and ore minerals from various stages are interpreted to have resulted from an evolutionary trend from hypersaline magmatic fluids during prograde skarn formation associated with Fe–As(–Ni) mineralization to low-salinity and low-temperature fluids during the retrograde skarn formation, associated with W–Cu–Zn mineralization. As the influence of magma-derived fluids waned, surficial fluids descended to deeper levels along fractures, resulting in siderite–quartz deposition associated with Zn–Pb–Ag mineralization. These results demonstrate that the Ulsan deposit is likely a skarn deposit that is genetically related to a low-sulfidation porphyry system.

Keywords: arsenopyrite, geothermometry, Fe–W skarn, polymetallic, fluid evolution, fluid inclusions, low sulfidation, Ulsan, southeastern Korea.

SOMMAIRE

La gisement de fer et de tungstène d'Ulsan est située dans le bassin volcano-sédimentaire crétacé de Gyeongsang, près de la bordure sud-est de la péninsule coréenne. Des événements hydrothermaux distincts ont mené à la formation d'un skarn calcique et des veines minéralisées dans un calcaire recristallisé, l'encaissant d'un pluton granitique épizonal d'âge tertiaire. Les gisements exploités à Ulsan fournissent une occasion unique de documenter l'évolution géochimique complexe d'un système de skarns et de veines lié génétiquement à un système à faible taux de sulfuration. Un métamorphisme de contact isochimique a produit un premier skarn (stade I) contenant des minéraux anhydres à Ca–Al–Mg au contact entre granite et calcaire recristallisé. Suite à la déposition de magnétite au stade principal de skarnification prograde (stade II), il y a eu un premier épisode de déposition d'arsénopyrite en intercroissance avec rammelsbergite – niccolite – gersdorffite – löllingite – bismuth natif – bismuthinite – pyrrhotite hexagonale. Ces assemblages de sulfures courants témoignent d'un état de faible sulfuration généralisé pendant la skarnification principale. Les skarns rétrogrades (stade III) contiennent des imprégnations mineures de scheelite dans la calcite et le quartz, avec actinolite et chlorite. Au cours de la partie ultime du stade III, les sulfures Cu–Zn et polymétalliques ont été introduits. Le dernière épisode du système hydrothermal (stade IV) a mené à une minéralisation Zn–Pb–Ag associée à des veines de sidérite–quartz. Une diminution des teneurs en As dans l'arsénopyrite en allant du stade II au stade IV indique une diminution en température ou en fugacité du soufre (ou les deux) avec le temps. Les divers événements de skarnification et les assemblages de minéraux de minerais des divers stades auraient résulté d'une évolution impliquant d'abord des fluides hypersalins magmatiques au cours de la skarnification prograde, associés à la minéralisation Fe–As(–Ni), et ensuite des fluides à faible salinité et faible température au stade rétrograde, associés à la minéralisation W–Cu–Zn. Avec la diminution de l'influence des

fluides orthomagmatiques, les fluides de surface ont atteint des niveaux profonds le long de fissures, pour déposer l'association sidérite–quartz avec minéralisation en Zn–Pb–Ag. D'après ces résultats, le gisement d'Ulsan semble être un skarn génétiquement lié à un système de porphyre à faible sulfuration.

(Traduit par la Rédaction)

Mots-clés: arsénopyrite, géothermométrie, skarn à Fe–W, polymétallique, inclusions fluides, évolution des fluides, faible sulfuration, Ulsan, Corée.

INTRODUCTION

Minerals of iron, tungsten, copper, zinc and lead occur in calcic skarns and hydrothermal vein deposits at the Ulsan mine, southeastern Korea. Skarn and ore mineralization developed as a result of multistage geochemical phenomena, which included silicate–oxide–sulfide metasomatism and subsequent hydrothermal alteration. Arsenopyrite is the most common sulfide mineral formed during the prograde metasomatic event through vein-filling episodes; it is closely associated with magnetite, scheelite, löllingite, native bismuth, bismuthinite, hexagonal pyrrhotite, pyrite and monoclinic pyrrhotite.

The successful application of the arsenopyrite geothermometer is only possible where arsenopyrite, sphalerite, löllingite and iron sulfides are deposited under equilibrium conditions, and where the arsenopyrite composition does not change during subsequent processes. The Ulsan mine presents an excellent opportunity to study arsenopyrite compositions with appropriate buffer assemblages to estimate changes in composition and temperature of the mineralizing fluids during ore deposition.

The first objective of this study is to document the compositional variation of arsenopyrite formed at different stages of mineralization. The second aim is to elucidate the nature and evolution of the physicochemical environment of ore deposition.

GEOLOGICAL SETTING AND DESCRIPTION OF THE ORE DEPOSIT

The Ulsan mine is located within the Cretaceous Gyeongsang Basin at the southeastern edge of the Korean Peninsula (Fig. 1). Mixed sequences of post-orogenic, molasse-type sedimentary rocks are intercalated with volcaniclastic rocks and lavas (the Hayang and Yucheon groups) in the basin. These Cretaceous sedimentary and volcanic rocks unconformably overlie highly deformed Precambrian crystalline basement of the Yeongnam Massif. The Middle Cretaceous to early Paleogene Bulgugsa suite of granitic rocks ranges from tonalite and granodiorite through granite to alkali-feldspar granite, and is predominantly of the magnetite series (Lee *et al.* 1987). These granitic rocks are epizonal and invariably display characteristics of subvolcanic

emplacement (Jin *et al.* 1981, Choi & Wee 1994). The Bulgugsa intrusive suite and volcanic rocks of the Hayang and Yucheon groups are considered to be comagmatic, subduction-related complexes (Lee *et al.* 1987). Within the Gyeongsang Basin, felsic volcanic rocks and granites at the southeastern margin are related closely to various types of copper, iron and tungsten deposits (Jin *et al.* 1981, Woo *et al.* 1982, Park *et al.* 1985).

At the Ulsan mine, recrystallized limestone and partially serpentinized ultramafic rocks (dunite and harzburgite) are exposed as a small roof pendant within the Upper Cretaceous sequence and intruding granitic rocks. Although the ages of both the ultramafic rock and recrystallized limestone are unknown, they are considered to represent the basement of the Cretaceous volcano-sedimentary piles in the study area. The Early Tertiary Gadae-Ri hornblende–biotite granite intruded the center of a dome structure located in the western part of the mine area (Fig. 1). Its biotite yields a K–Ar age of 58 and 62.9 ± 1.9 Ma (Lee & Ueda 1977, Reedman *et al.* 1989). In spite of the spatial separation (<100 m) between the mineralized zones and the Gadae-Ri granite stock, the ore deposits are considered to be related genetically to this pluton (Choi & Imai 1993).

The calcic Fe–W skarn deposit at Ulsan occurs as a nearly vertical ore pipe within recrystallized limestone at the direct contact with the Upper Cretaceous volcanic rocks containing thin layers of pelitic sedimentary rocks. Ore minerals consist mainly of magnetite and lesser amounts of scheelite with minor sulfides, arsenides, sulfosalts and sulfarsenides. The formation of the ore pipe seems to be controlled by the intersection of two structural elements: (1) east–west-trending, steeply dipping stratigraphic contacts between recrystallized limestone and the overlying intercalated Cretaceous volcanic and sedimentary rocks, and (2) north–south-trending high-angle fractures now occupied by parallel andesitic dykes.

SKARN EVOLUTION AND MINERALIZATION

Skarn development and ore mineralization in the Ulsan deposits are the results of complex, multistage geochemical phenomena. The sequential deposition of minerals has been determined from cross-cutting features, replacement textures, relationships among miner-
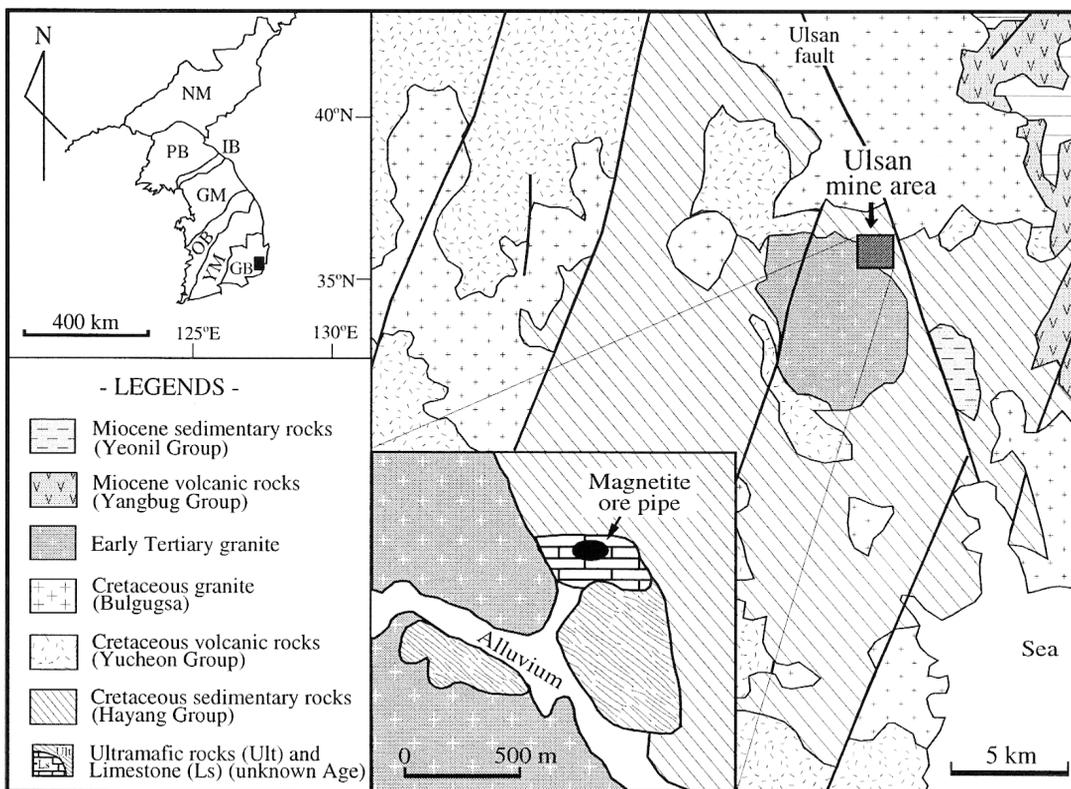
FIG. 1.   Geological map of the Ulsan mine area showing the detailed map of the mining geology. The location of the Ulsan mine area (shaded box) is shown on the inset map of the Republic of Korea. GB: Gyeongsang Basin, GM: Gyeonggi Massif, IB: Imjingang Belt, NM: Nangrim Massif, OB: Ogcheon Belt, PB: Pyongnam Basin, YM: Yeongnam Massif.

als and mineral assemblages. Skarn formation and mineralization due to the emplacement of the Gadae-Ri granite took place in four distinct stages; the paragenetic episodes of skarn and ore mineralogy are summarized in Figure 2.

During stage I, skarn formation began with a highly calcic assemblage represented by diopside + wollastonite + grossular + vesuvianite at the granite–marble contact. This stage did not involve ore minerals.

Prograde metasomatic skarn formation during stage II is divided into two substages (IIa and IIb) depending on whether the predominant ore mineral is magnetite or arsenopyrite. Skarn minerals formed at high temperature during the main prograde event (substage IIa) are characterized by fine-grained anhydrous calc-silicates, magnetite and calcite. Clinopyroxene is, however, the volumetrically most important mineral. The early fine-grained phases were followed by formation of medium-grained clinopyroxene with 5.3–48.6 mole % hedenbergite and a grandite-type garnet with intermediate compositions (10.4–82.4 mole % andradite). The main

Fe mineralizing event, which played an important role in the development of bodies of massive magnetite in the ore pipe, took place in the middle period of this skarn stage. During latest part of stage IIa, veins that crosscut earlier assemblages of skarn minerals consist of coarse-grained clinopyroxene and garnet that become progressively more iron-enriched and magnesium-depleted. At the beginning of substage IIb, minor amounts of niccolite, rammelsbergite, löllingite, gersdorffite, arsenopyrite, and native bismuth were deposited with calcite and minor quartz. The Fe–As(–Ni) association is present mainly as massive and disseminated ores with skarn minerals, magnetite and calcite within the magnetite ore pipe and the surrounding calcite zone.

During stage III (retrograde skarn stage), hydrous alteration of pre-existing skarn minerals occurred, involving for example the alteration of clinopyroxene to calcic amphibole, with chlorite, ilvaite, epidote, calcite and quartz. Scheelite as a byproduct overgrew and replaced magnetite and calc-silicates within the ore pipe during substage IIIa. Copper–zinc and polymetallic

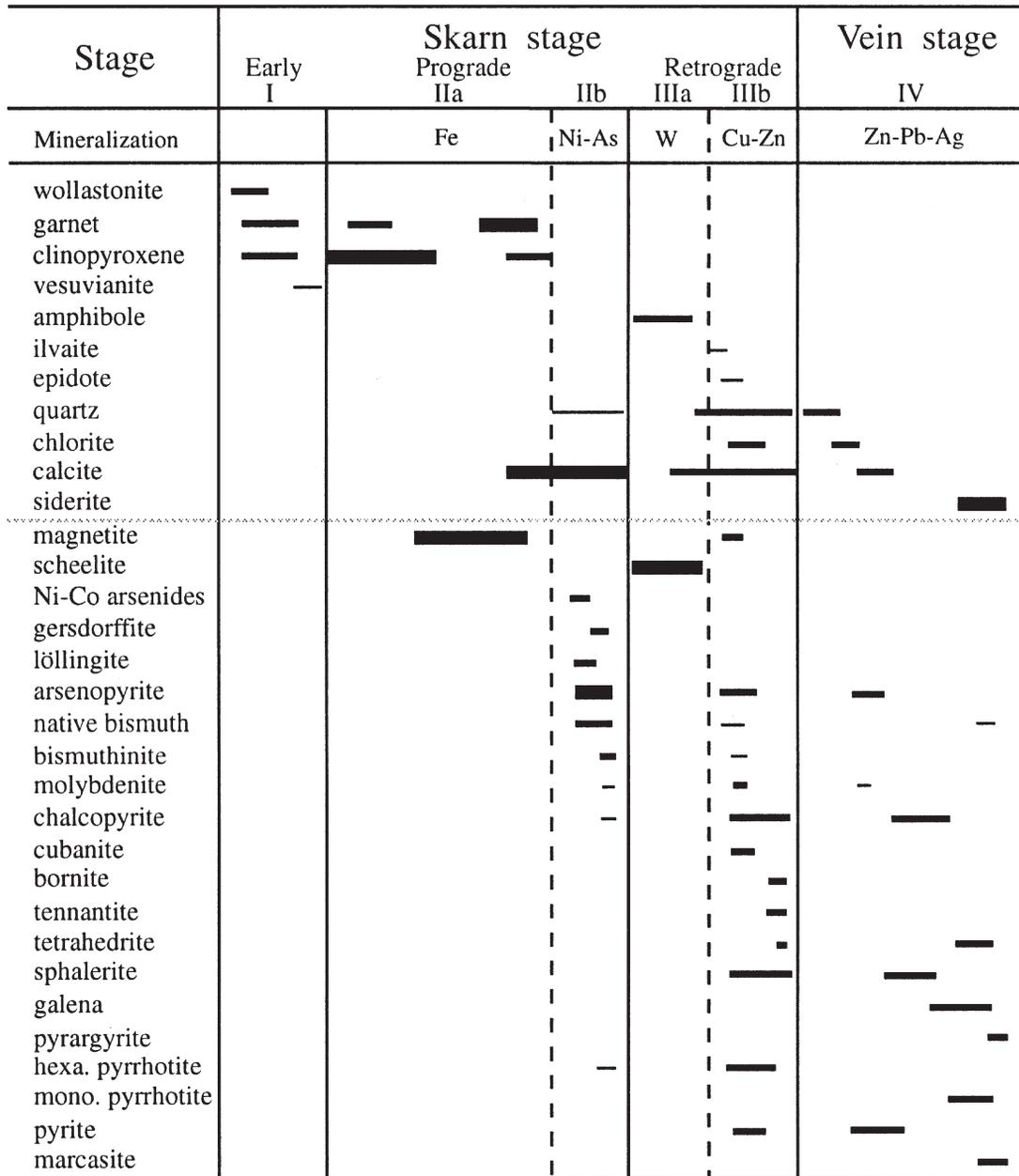| Stage	Skarn stage					Vein stage
	Early I	Prograde IIa	IIb	Retrograde IIIa	IIIb	IV
Mineralization		Fe	Ni-As	W	Cu-Zn	Zn-Pb-Ag

FIG. 2. Simplified paragenetic sequences for the assemblages of principal ore and alteration minerals at Ulsan mine. Line thicknesses represent schematically the relative abundances of the mineral deposited.

mineralization overprinted previous tungsten mineralization during substage IIIb. Substage IIIb is also represented by the crystallization of chalcopyrite, sphalerite, hexagonal pyrrhotite, pyrite, arsenopyrite, cubanite, bornite, chalcocite and bismuthian tennantite, with minor or trace amounts of bismuth, bismuthinite, roquesite, tetrahedrite, cobaltite, wittichenite, miharaite, hessite, mawsonite and aikinite, although these ore minerals are present in minor or trace amounts. Substages IIIa and IIIb are successive, and must be regarded as resulting from a single event.

Stage IV represents the formation of fissure-controlled veins that clearly cut the Fe–W ore pipe and surrounding skarns. This stage represents the latest phase of hydrothermal Zn–Pb–Ag mineralization superimposed on the skarn alteration described previously. The Zn–Pb–Ag association occurs in veins of siderite – quartz – chlorite gangue with galena, sphalerite, pyrite, arsenopyrite, monoclinic pyrrhotite, and minor amounts of chalcopyrite, molybdenite, Ag-bearing tetrahedrite, pyrargyrite, polybasite, gudmundite and marcasite. It is volumetrically insignificant and is uneconomic.

TYPES OF ARSENOPYRITE

Arsenopyrite-bearing ores formed during the various stages of mineralization have been examined, and

TABLE 1. DESCRIPTION OF THE ORE SPECIMENS
FROM THE ULSAN MINE

Specimen no.	Ore type	Stage	Ore-mineral assemblage	Occurrence
U532-2	Ni-As	II	Gf,Nc,Rm,Lol,Apy,Bi	disseminated
U338-1	Ni-As	II	Gf,Nc,Lol,Rm,Apy,Bi	disseminated
U316	Ni-As	II	Gf,Apy,Lol,Bi,Mlb	disseminated
U840516	As	II	Apy,Lol,Bi,Po-I,Ccp	disseminated
U840508	As	II	Apy,Lol,Bi	massive
U1022C	As	II	Apy,Lol,Bi	massive
U830113	Fe-As	II	Mgt,Apy,Lol,Bi	disseminated
U733B	Fe-As	II	Mgt,Apy,Lol,Bi	disseminated
UB81-2-2	As	II	Apy,Lol,Bi	massive
U807	As	II	Apy,Bi	massive
UB81-2-8-3F	As	II	Apy,Lol,Bi	massive
U106	As	II	Apy,Bi,Bm	massive
U101	As	II	Apy,Bi,Bm	massive
UB81-3-3A	As	II	Apy,Bi,Bm	massive
U840518A	As	II	Apy,Lol,Bi,Po-I,Bm,Py	massive
UB830113A	Fe-W-As	II, III	Mgt,Sch,Bm,Bi,Po-I,Apy,Ccp	dissem.
UB830105	Fe-Cu-Zn	II, III	Mgt,Sp,Ccp,Po-I	disseminated
UB830107	Fe-Cu-Zn	II, III	Mgt,Ccp,Po-I,Sp	disseminated
U96D	Fe-Cu-Zn-W	II, III	Mgt,Po-I,Py,Ccp,Sp,Apy,Sch	dissem.
U96B	Fe-Cu-Zn	II, III	Mgt,Po-I,Py,Ccp,Sp,Apy	disseminated
U820880	Fe-W-Cu-Zn	II, III	Mgt,Sch,Py,Po-I,Apy,Bi,Bm,	stringer
			Lol,Po-II,Ccp,Sp,Cb,Bn	
U840505A	Cu	III	Po-I,Py,Ccp,Apy,Mc,Po-II	stringer
U840505B	Cu-Zn	III	Po-I,Py,Ccp,Sp,Apy,Po-II	stringer
U850307A	Cu-Zn	III	Ccp,Sp,Po-I,Po-II,Py,Td,Mc,Gn	dissem.
UB81-3-4D	W-Cu-Zn	III	Sch,Bn,Sp,Ccp,Cc,Tn,Wi,Hs,Co	stringer
U535	Zn-Cu	III	Sp,Ccp,Py,Bn	disseminated
U9001	Zn-As	III	Py,Po-II,Sp,Apy,Ccp,Mc	stringer
U94	Zn-As-Cu	IV	Py,Po-II,Apy,Sp,Ccp,Bm,Td	dissem.
U95C	As	IV	Po-II,Apy,Py,Ccp	quartz vein
U94-291	As	IV	Apy,Py	quartz vein
U97	As	IV	Py,Apy,Po-II,Ccp	disseminated
U600A	Zn-Pb-Ag	IV	Py,Bm,Bi,Sp,Gn,Apy,Pg,Pl,Ccp	Sd–Qtz
U600B	Zn-Pb-Ag	IV	Py,Po-II,Sp,Gn,Apy,Ccp,Mc,Td	Sd–Qtz
U1013B	As-Zn	IV	Py,Apy,Po-II,Sp,Ccp,Mc	Chl–Qtz
U709	Zn-Pb	IV	Po-II,Py,Sp,Ccp,Apy,Gn,Mlb	Chl–Qtz
U850306-2A	Zn-Pb	IV	Po-II,Py,Sp,Gn,Mc,Apy	quartz vein
UB8004-1	Zn-Pb	IV	Py,Sp,Gn,Mc,Apy	Sd–Qtz
UB8004-4	Zn-Pb	IV	Py,Po-II,Mc,Gn,Sp,Apy	Sd–Qtz

Symbols in the last column: Sd–Qtz: siderite–quartz vein, Chl–Qtz: chlorite–quartz vein. Mineral symbols: Apy: arsenopyrite, Bi: native bismuth, Bm: bismuthinite, Bn: bornite, Cb: cubanite, Cc: chalcocite, Ccp: chalcopyrite, Co: cobaltite, Gf: gersdorffite, Gn: galena, Hs: hessite, Lol: löllingite, Mc: marcasite, Mgt: magnetite, Mlb: molybdenite, Nc: niccolite, Pg: pyrargyrite, Pl: polybasite, Po-I: hexagonal pyrrhotite, Po-II: monoclinic pyrrhotite, Py: pyrite, Rm: rammelsbergite, Sch: scheelite, Sp: sphalerite, Td: Ag-bearing tetrahedrite, Tn: tennantite, Wi: wittichenite.

three episodes of arsenopyrite deposition were recognized. Ores containing arsenopyrite are present mainly as massive and disseminated sulfides intergrown with skarn minerals, and as stringer and subordinate veins with quartz, siderite and chlorite (Table 1). Although these sulfides are more abundant in the outer calcite-rich zone than in the magnetite-dominant ore zone, there is no systematic lateral zonation of mineral assemblages. Arsenopyrite is subdivided into five groups on the basis of texture, relationships with gangue minerals, and coexisting Fe–As–S minerals. The groups are described as arsenopyrite A, B, C, D and E throughout the text, figures, and tables.

The first generation of arsenopyrite, formed during the prograde skarn of stage II, is present mainly as disseminated, fine-grained particles or massive aggregates distributed within magnetite ore, skarn and calcite. Such arsenopyrite has been divided into three groups, depending on whether the predominant opaque phase is Ni–Co arsenide (arsenopyrite A), Fe arsenide (arsenopyrite B) or native bismuth – bismuthinite (arsenopyrite C). Arsenopyrite A tends to occur as discrete grains (100–200 μm) with an irregular outline; it is erratically distributed in various types of skarn. Arsenopyrite A fills the interstices between calc-silicate aggregates, consisting commonly of clinopyroxene + grandite garnet. It is intergrown intimately with niccolite, rammelsbergite, gersdorffite, löllingite and native bismuth. Arsenopyrite overgrew and replaced niccolite or gersdorffite, and locally contains gersdorffite remnants in the core. Arsenopyrite A also occurs as euhedral to subhedral rhombs whose rim has lower concentrations of Ni and Co. Although this compositional zoning cannot be recognized optically, it is easily recognized in back-scattered electron images. Most grains of arsenopyrite B and C occur in massive As-rich ores distributed within the Fe–W ore pipe and in the outermost calcite zone (Choi & Imai 1985).

The most common and characteristic sulfides associated with first-generation arsenopyrite at the Ulsan mine are native bismuth – löllingite – arsenopyrite B and native bismuth – bismuthinite – arsenopyrite C. Arsenopyrite B is intergrown intimately with löllingite lamellae and native bismuth. Arsenopyrite C contains spindle- or wedge-shaped inclusions consisting of both native bismuth and bismuthinite. These textural relations indicate the simultaneous equilibrium crystallization of arsenopyrite B with löllingite and native bismuth, and of arsenopyrite C with bismuthinite and native bismuth. In some samples (e.g., U840518A), signs of replacement and corrosion of arsenopyrite by pyrite are present locally, indicating the later deposition of pyrite.

The second generation, arsenopyrite D, formed during the complex polymetallic mineralization of stage IIIb. In the main Cu–Zn sulfide stage, arsenopyrite D is intergrown with hexagonal pyrrhotite, pyrite, chalcopyrite and sphalerite. Euhedral arsenopyrite and pyrite coexist with pyrrhotite, suggestive of coprecipitation.

Chalcopyrite displays exsolution textures with fine lamellae of cubanite, hexagonal pyrrhotite, and star-shaped sphalerite. Hexagonal pyrrhotite was partly altered to monoclinic pyrrhotite and marcasite, particularly along fractures and grain boundaries. In this study, the distinction between hexagonal and monoclinic pyrrhotite was determined by X-ray diffractometry and the magnetic colloidal suspension method (Craig & Vaughan 1994).

The third generation, arsenopyrite E, was formed during Zn–Pb–Ag mineralization (stage IV), which comprises pyrite, sphalerite, galena, monoclinic pyrrhotite and Ag-bearing sulfosalts, with siderite and quartz. Arsenopyrite E generally occurs as euhedral to subhedral grains and appears texturally to be coprecipitated with pyrite and sphalerite. In addition, monoclinic pyrrhotite and Ag-bearing sulfosalts fill interstices among grains of arsenopyrite, sphalerite and pyrite, open fractures, and the opened cleavage of galena.

Composition of Arsenopyrite and Sphalerite

Arsenopyrite, sphalerite, löllingite, pyrite and pyrrhotite were analyzed with a JEOL JXA–8600 Superprobe with energy-dispersion and wavelength-dispersion spectrometers at the Center for Mineral Resources Research (CMR), Korea University. The instrument was operated at an accelerating voltage of 20 kV and a beam current of 30 nA. Special attention was paid to quantitative analysis of the samples for arsenic. The As contents were invariably checked using two ultrapure standards (InAs and GaAs). Also, emphasis was placed on selecting arsenopyrite and sphalerite grains in mutual

contact with iron sulfides or iron arsenide, and investigating the homogeneity of these grains. Raw data were corrected using the Oxford ZAF matrix-correction program. Analytical totals accepted for this study are between 98.5 and 101.0 wt.%.

Arsenopyrite

Over 300 spot analyses were made on arsenopyrite from three different stages of mineralization, and several grains were analyzed in the same polished section. In addition to the main components of arsenopyrite, Ni, Co, and Sb also were sought (Table 2). Although there is a wide range in chemical composition of arsenopyrite, especially in terms of As, S, Ni and Co, in almost all cases, with the exception of arsenopyrite A, individual grains are typically homogeneous.

Arsenopyrite A (Ni–Co-bearing species) is associated with niccolite, rammelsbergite, löllingite, and gersdorffite, deposited during stage IIb. It contains up to 10.0 wt.% Ni, and higher As and Co contents than the other types of arsenopyrite. The analyses indicate that arsenopyrite A is strongly zoned; a striking enrichment in As in the core is correlated with an increase in Ni and Co contents. Ni and Co are also present as minor elements in the coexisting löllingite (up to 1.8 and 4.0 wt.%, respectively). The total concentration of Ni and Co in most grains of arsenopyrite does not exceed 1 wt.% (Fig. 3). The variation in iron content of most grains of arsenopyrite at Ulsan is insignificant: 33.3 ± 0.7 atomic %.

In contrast, the arsenopyrite may exhibit extreme chemical variations in As and S. The range of As con-

TABLE 2. REPRESENTATIVE CHEMICAL COMPOSITIONS OF LÖLLINGITE, ARSENOPYRITE, AND PYRITE FROM THE ULSAN MINE

Species	1 Löllingite	2	3	4	5 Arsenopyrite	6	7	8	9	10	11 Pyrite
Stage	IIb	IIb	IIb	IIb	IIb	IIb	IIIb	IIIb	IV	IV	IV
Anal. #	7	5	2	8	7	9	18	6	17	18	5
Fe wt.%	28.87	26.62	27.17	33.64	34.00	34.93	34.41	34.66	34.62	35.33	45.76
Co	0.00	0.17	0.65	0.00	0.08	0.04	0.00	0.00	0.00	0.00	0.00
Ni	0.00	0.69	5.45	0.00	0.04	0.00	0.00	0.01	0.00	0.00	0.11
As	69.49	70.79	50.38	47.55	46.92	46.59	44.68	45.14	44.86	42.44	1.84
S	1.98	1.44	15.89	18.14	18.55	18.89	20.31	20.08	20.79	21.56	51.95
Sb	0.00	0.00	0.03	0.00	0.00	0.00	0.00	0.00	0.00	0.03	0.00
Total	100.34	99.72	99.56	99.33	99.60	100.44	99.41	99.94	100.28	99.37	99.66
Fe at.%	34.32	32.17	27.67	33.41	33.53	34.04	33.37	33.56	33.20	33.80	33.22
Co	0.00	0.19	0.62	0.00	0.08	0.03	0.00	0.00	0.00	0.00	0.00
Ni	0.00	0.80	5.28	0.00	0.03	0.00	0.00	0.01	0.00	0.00	0.13
As	61.58	63.79	38.24	35.20	34.49	33.85	32.31	32.57	32.07	30.26	1.00
S	4.10	3.03	28.18	31.38	31.86	32.07	34.32	33.86	34.73	35.92	65.70
Sb	0.00	0.00	0.01	0.00	0.00	0.00	0.00	0.00	0.00	0.01	0.00

Note: 1: UB81-2-2; 2, 4: U840508; 3: U338-1; 5: U830113; 6: UB81-3-3A; 7: U840505B; 8: U96B; 9: U600A; 10: UB8004-4, 11: U840518A. 0.00: below detection limit.
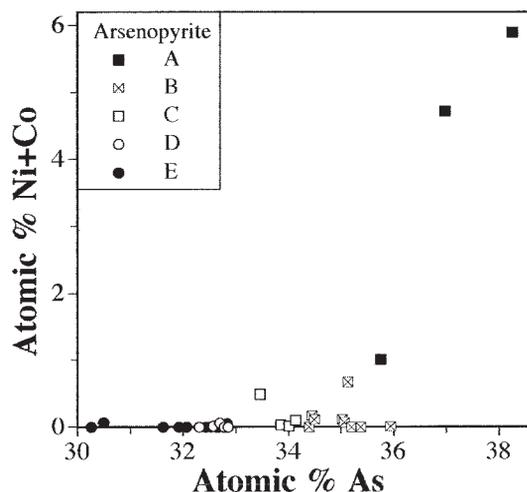

FIG. 3. The average content of Ni + Co (atomic %) and As (atomic %) in arsenopyrite from the samples studied. Note the very high Ni + Co content of arsenopyrite A.

tents and the average for all grains analyzed are shown in Table 3. The arsenic contents of each specimen show a narrow compositional variation (<1.5 atomic %). The compositional variation within a single grain is normally less than the variation among different grains from the same polished section. All arsenopyrite grains that show >1 atomic % As variation in core–rim pairs were rejected for geothermometry.

The chemical compositions of arsenopyrite reveal that there is a consistent relationship between arsenic and sulfur on one hand and mineral assemblage (Fig. 4, Table 3). Arsenic and sulfur are strongly negatively correlated, following roughly the classical substitution: $FeAs_{1\pm x}S_{1\pm x}$. The consistency implies chemical equilibrium during the formation of various stages of mineralization (Fig. 5). However, arsenopyrite grains in some specimens (U840518A, UB830113A and U820880) seem to be compositionally more variable than others. The conspicuous presence of pores in the margins of some grains indicates that they subsequently underwent chemical overprinting by retrograde reaction or dissolution. This textural evidence reflects varying degrees of retention of equilibrium; data from such grains of arsenopyrite are not considered reliable for geothermometric purposes.

Sphalerite

At least two generations (retrograde skarn and vein stage) of sphalerite are recognized from the Cu–Zn and Zn–Pb–Ag ores. Sphalerite is present mainly in dissemi-

FIG. 5. Frequency distribution of As content (atomic %) in arsenopyrite of different stages and different assemblages from the Ulsan mine. See Table 1 for mineral abbreviations.
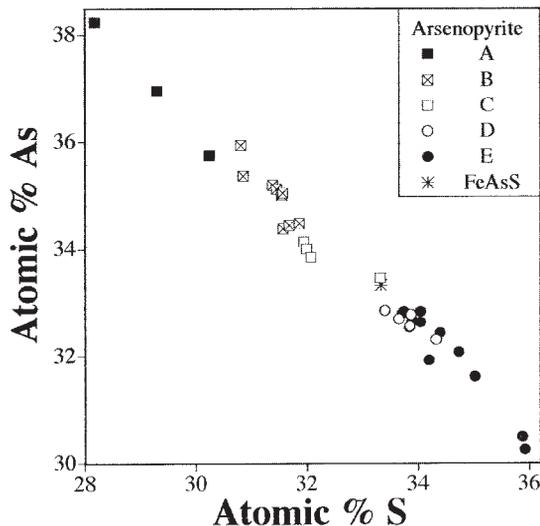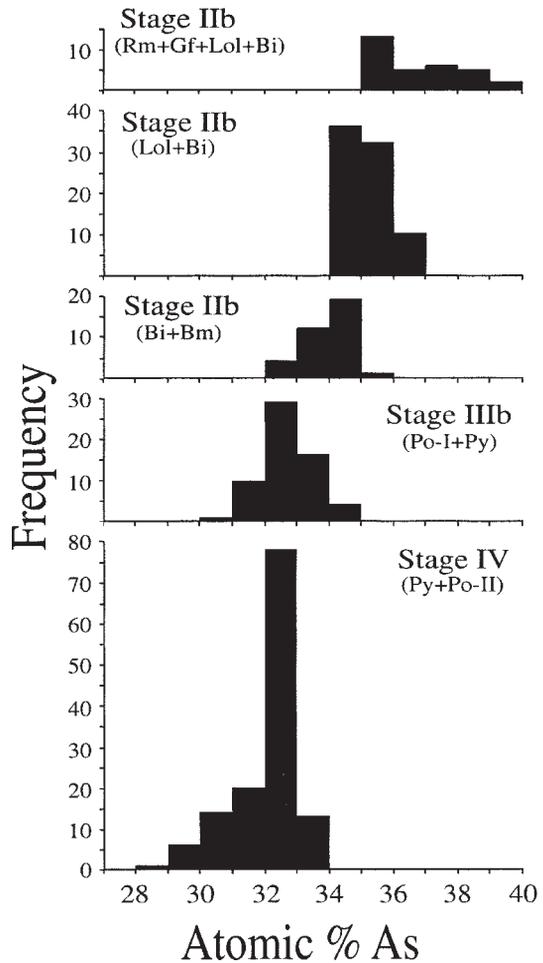

FIG. 4. The average content of S and As (atomic %) in arsenopyrite from samples studied. Note the wide variation of As content in arsenopyrite as a function of different assemblages (A though E).

nated or massive ores accompanying hydrous silicates, and in stringer and subordinate veins with quartz, siderite and chlorite. Chemical compositions of sphalerite were determined in order to define more precisely the T–X conditions of ore formation (Table 4), as the cogenetic sulfides (arsenopyrite, sphalerite and chalcopyrite) possess a wide field of stability. Only small or negligible amounts of Cd, Cu, In and Mn were detected.

The Cu–Zn ore developed in stage IIIb is classified into two groups on the basis of the mineral species present: Cu–Zn (I) and polymetallic Cu–Zn (II). The Cu–Zn associations may have formed after the deposition of the scheelite and vuggy quartz, together with calcite, at the end of stage IIIb. Electron-microprobe

TABLE 3. AVERAGE AND RANGE (ATOMIC %) OF As CONTENT IN TYPES OF ARSENOPYRITE ASSOCIATED WITH DIFFERENT SULFIDE ASSEMBLAGES

Specimen	Atomic % As				Estimated Temperature (°C)	Types of Apy
	Average	S.D.*	Range	N**		
U532-2	36.97	1.28	35.02-39.80	20	not available	A
U338-1	38.24	0.77	37.47-39.01	2	not available	A
U316	35.75	0.56	35.24-36.76	9	not available	A
U840518A	35.94	0.58	34.98-36.96	13	not available	A,B,C
U840516	35.06	0.45	34.24-35.74	13	500 ± 40	B
U840508	35.20	0.32	34.43-35.52	8	510 ± 30	B
U1022C	35.02	0.52	34.28-36.09	12	500 ± 50	B
U830113	34.49	0.32	34.02-35.08	7	470 ± 25	B
U733B	34.45	0.17	34.17-34.69	5	470 ± 15	B
UB81-2-2	34.39	0.33	34.06-34.93	4	465 ± 25	B
U807	35.37	0.47	34.72-36.19	8	520 ± 40	B
UB81-2-8-3F	35.13	0.67	34.13-36.18	8	505 ± 55	B
U106	34.14	0.33	33.64-34.54	10	475 ± 25	C
U101	34.01	0.39	33.30-34.52	10	470 ± 35	C
UB81-3-3A	33.85	0.31	33.33-34.15	9	460 ± 25	C
UB830113A	33.46	1.26	32.01-35.08	7	not available	C,D
U96D	32.78	0.53	32.12-33.36	5	470 ± 45	D
U840505A	32.70	0.47	31.78-33.14	6	465 ± 45	D
U96B	32.57	0.50	32.05-33.30	6	455 ± 45	D
U840505B	32.31	0.49	31.23-32.94	18	435 ± 55	D
U820880	32.86	0.99	30.94-34.34	23	not available	B,D
U9001	32.67	0.36	32.03-32.21	14	460 ± 40	E
U94	32.44	0.39	31.49-32.91	14	445 ± 45	E
U95C	32.54	0.19	32.33-32.88	7	450 ± 20	E
U94-291	32.84	0.14	32.69-33.10	8	470 ± 20	E
U97	32.64	0.31	32.08-33.23	17	460 ± 40	E
U600A	32.07	0.34	31.59-32.57	17	420 ± 30	E
U600B	32.80	0.34	32.24-33.20	8	470 ± 35	E
U1013B	32.84	0.35	32.22-33.26	10	470 ± 40	E
U709	31.92	0.36	31.22-32.27	8	410 ± 30	E
U850306-2A	31.62	0.47	30.74-32.10	6	390 ± 40	E
UB8004-1	30.50	0.62	29.76-31.22	5	325 ± 50	E
UB8004-4	30.26	0.61	28.46-31.23	18	310 ± 90	E

* Standard deviation.
** Number of spot analyses by electron microprobe.

TABLE 4. AVERAGE AND RANGE OF FeS CONTENTS IN SPHALERITE FROM STAGES III AND IV, ULSAN DEPOSIT, SOUTHEASTERN KOREA

Specimen no.	Mole % FeS				Assoc. Apy
	Average	S.D.*	Range	N**	
UB830105	21.54	0.42	20.67-22.08	7	-
UB830107	20.68	0.78	19.41-21.90	10	-
U850307A	18.16	0.37	17.30-18.65	15	-
U96D	17.42	0.21	17.07-17.76	6	D
U840505B	17.91	0.26	17.56-18.34	5	D
U820880	5.29	4.84	1.52-17.25	27	B,D
UB81-3-4D	0.44	0.13	0.28-0.71	16	-
U535	1.83	0.14	1.65-2.15	11	-
U9001	16.78	0.83	15.18-17.59	7	E
U600A	17.22	0.31	16.78-17.81	12	E
U600B	18.55	0.38	18.08-19.34	9	E
U1013B	16.33	0.74	14.95-17.20	10	E
U709	15.93	0.78	14.23-16.64	9	E
U850306-2A	17.74	0.49	16.73-18.22	6	E
UB8004-1	17.96	0.81	15.80-19.61	16	E
UB8004-4	18.20	0.27	17.82-18.65	6	E

* Standard deviation. -: absent.
** Number of spot analyses by electron microprobe.

results show that sphalerite intergrown with chalcopyrite, hexagonal pyrrhotite and pyrite in Cu–Zn (I) ore contains 17.1 to 18.7 mole % FeS (Fig. 6). Sphalerite intergrown only with chalcopyrite and hexagonal pyrrhotite is generally more iron-rich (19.4 to 22.1 mole % FeS). Such restricted iron contents are typical of sphalerite deposition along the hexagonal pyrrhotite – pyrite buffer equilibrium. The beginning of this sulfide deposition, therefore, took place over a range of $f(S_2)$, around $10^{-6.0}$ to $10^{-5.2}$ atm at 450°C. The bimodal distribution of FeS content in sphalerite from specimen no. U820880 is similar to the wider compositional variation of As content in arsenopyrite (Tables 3, 4). This result is consistent with the presence of the association löllingite – bismuthinite – pyrite – bornite – tennantite – pyrrhotite, suggestive of a disequilibrium association. Overprinting of earlier compositions by later ore fluids helps to explain the formation of unusual compositions of both sphalerite and arsenopyrite.

The polymetallic Cu–Zn (II) ore obtained from drill core was found only at the innermost contact zone between granite and recrystallized limestone. Bornite, sphalerite, chalcopyrite, chalcocite and tennantite are abundant, and sulfosalts of Cu and Ag tellurides also occur. The composition of sphalerite without pyrrhotite or pyrite is iron-poor (0.3 to 2.2 mole % FeS). During the latest part of stage IIIb, the appearance of bornite, chalcopyrite, chalcocite and tennantite, and then iron-poor sphalerite in Cu–Zn (II) ore, implies a shift to higher $f(S_2)$ conditions outside the stability field of pyrrhotite. The high sulfidation assemblage in the Cu–Zn (II) ore may be interpreted to indicate that ore fluids evolved locally as a result of repeated emanations of magmatic fluid from the nearby granite. Sphalerite throughout stage IIIb formed at similar temperatures as massive or disseminated ores, but with quite different mineral assemblages, firstly sulfide-rich Cu–Zn (I), with chlorite – quartz – calcite, then polymetallic sulfide-rich Cu–Zn (II), with quartz – calcite.

Sphalerite in Zn–Pb–Ag ores from stage IV, which is iron-rich (14.2 to 19.6 mole % FeS), is found in assemblages dominated by pyrite, sphalerite, galena, marcasite, monoclinic pyrrhotite and Ag-bearing sulfosalts with siderite and quartz. Deposition of these minerals appears to have begun within the stability field of pyrite and continued into that of monoclinic pyrrhotite. The end of the vein stage occurred at conditions of lower $f(S_2)$, in the stability field of siderite. Such changes in composition of the ore fluid could reflect several different processes, including changes in temperature and composition of the ore fluid or mixing of fluids with time.

FLUID INCLUSIONS

Fluid inclusions in skarn and vein minerals from various stages of mineralization were studied in order
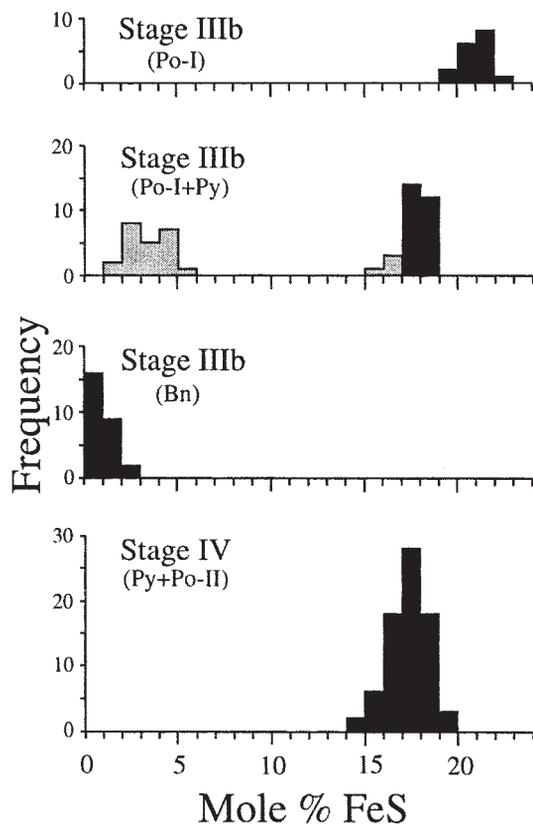
FIG. 6. Frequency distribution of FeS contents (mole %) in sphalerite of different stages and different assemblages from the Ulsan mine. Note the gap (shaded area) of FeS content (mole %) in sphalerite from specimen no. U820880 in stage IIIb (Po-I + py). See Table 1 for mineral abbreviations.

to determine temporal variations in temperature and composition of ore-forming fluids. All fluid-inclusion measurements were made using doubly polished sections (100 μm thick) prepared from calcite, clinopyroxene, garnet, quartz, and scheelite. Microthermometric measurements were made on fluid inclusions using a U.S. Geological Survey gas heating and freezing system adapted by Fluid Inc. (Woods *et al.* 1981) calibrated with synthetic H_2O and CO_2 inclusions. Heating rates were maintained near 2°C/min for measurements of total homogenization temperatures (T_h-total). During freezing experiments, a sequential technique of freezing (Haynes 1985) was employed. Salinity data are based on freezing-point depression in the system H_2O–NaCl (Potter *et al.* 1978) for CO_2-absent, aqueous inclusions (types I and II), on clathrate-melting tempera-

tures (Bozzo *et al.* 1975, Diamond 1992) for CO_2-bearing inclusions (type IV), and on the dissolution temperatures of daughter minerals (Chou 1987, Sterner *et al.* 1988) for daughter-mineral-bearing inclusions (type III). The reproducibility of measurements was ±1.0°C for T_h-total values and melting temperatures of halite (T_m-NaCl). Homogenization temperatures of the CO_2 phase (T_h-CO_2) and melting temperatures of CO_2 phases (T_m-CO_2), ice (T_m-ice), and clathrate (T_m-clath.) have errors of ±0.2°C.

Types of fluid inclusions

Fluid inclusions were subdivided into four types on the basis of phase relations at 20°C and microthermometric behavior during cooling and heating experiments. Type-I inclusions are two-phase and H_2O-rich inclusions with small vapor bubbles (<25 vol.%). Type-II inclusions are two-phase and H_2O-rich inclusions with large vapor bubbles (>80 vol.%). Type-III inclusions are polyphase daughter-mineral-bearing inclusions with small vapor bubbles (<35 vol.%). Type-IV inclusions are three-phase CO_2-bearing inclusions with liquid CO_2, vapor CO_2, and liquid water.

Fluid inclusions occur in a variety of minerals with various salinities and homogenization temperatures. In general, type-III inclusions occur only in minerals of the prograde skarn stage, forming the Fe–As mineralization, whereas inclusions of types I, II and IV occur in minerals of the retrograde skarn and vein stages that form the tungsten and polymetallic sulfide mineralization. The size of inclusions is variable (<10 to 150 μm), but ranges generally from 20 to 40 μm. Repeated fracturing and healing, both during and after mineral deposition, make it difficult to determine the relative chronology of fluid inclusions within skarn and vein minerals. However, in some cases, it was possible to establish a relative chronology of inclusions using the criteria of Roedder (1984). Several generations of fluid inclusions may be recognized from their textural relationships with respect to other assemblages of fluid inclusions. Most type-III inclusions are isolated, without planar array, and are regular in shape, suggestive of a primary origin. Some secondary type-III inclusions, however, occur along healed fractures. Type-I inclusions show a variety of forms ranging from irregular to rounded or negative-crystal shapes. Secondary type-I inclusions occur in planar arrays on the healed traces of fractures that cut the crystal boundaries. Type-II and type-IV inclusions are found in randomly distributed and isolated occurrences.

Fluid inclusions in the prograde metasomatic skarn-formation event (stage II) are found in clinopyroxene, garnet, calcite and quartz. The order of relative abundance is type III >> type I. No vapor-rich or CO_2-bearing inclusions were observed. Most inclusions in clinopyroxene, calcite and quartz are of type III, *i.e.*, daughter-bearing inclusions (Figs. 7A, B). They contain vapor bubbles comprising 15 to 35 vol.% and daughter
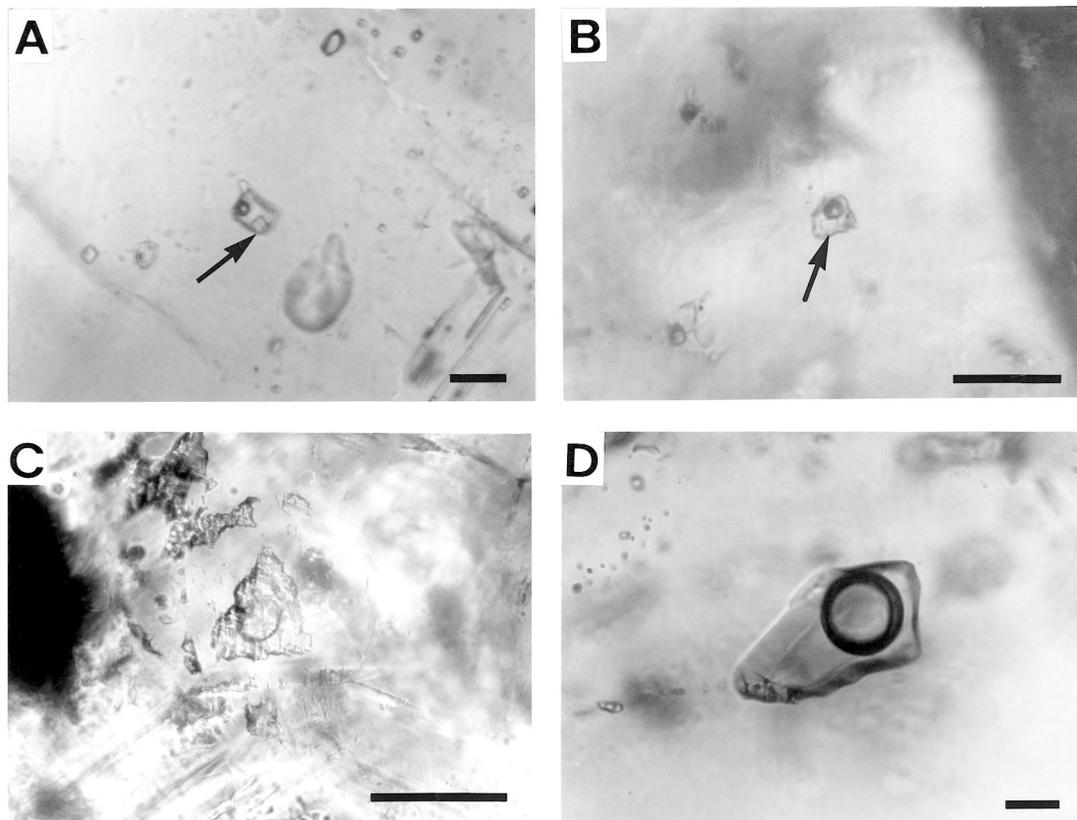
FIG. 7. Photomicrographs showing the types and occurrences of fluid inclusions in skarn and vein minerals from the Ulsan deposits. (A) Type-III hypersaline inclusion in stage-II calcite. (B) Type-III inclusion in stage-II clinopyroxene. (C) Type-I aqueous inclusion in stage-II garnet. (D) Type-IV CO_2-bearing inclusion in stage-III quartz. All scale bars are 25 μm. Arrows point to halite as a daughter mineral in type-III inclusions.

minerals comprising 10 to 25% of the inclusion volume, and homogenized by disappearance of vapor. The dominant solid in these inclusions is NaCl, though other unidentified daughter minerals are present.

Type-I aqueous inclusions are found in anisotropic garnet and in some coarse-grained euhedral crystals of clinopyroxene. Fluid inclusions in euhedral garnet, which fills the local fractures within magnetite ore, occur along growth zones and are assumed to be primary (Fig. 7C). Fluid inclusions in clinopyroxene and anisotropic garnet, trapped during the later period of stage IIa, are not sufficiently abundant for study.

Fluid inclusions in stage III occur in calcite, scheelite and quartz formed in retrograde skarn. The order of relative abundance is type I >> type IV > type II. Type-I inclusions contain vapor bubbles comprising 10 to 25 vol.%, homogenize readily to the liquid phase upon heating, and do not contain any daughter minerals. Only four type-II inclusions in quartz were recognized, and

they occur only in this stage. They contain vapor bubbles comprising 80 to 90 vol.% and homogenize to the vapor. Type-IV inclusions occur only as primary inclusions in quartz crystals (Fig. 7D) overgrown by chalcopyrite. They have variable CO_2 contents, even within individual samples. T_m-CO_2 values near –57°C indicate that the vapor bubbles are composed of nearly pure CO_2. The actual CO_2 content of the vapor, however, is not well constrained owing to difficulties in observing CO_2 liquid–vapor homogenization. These type-IV inclusions seem to be coeval with inclusions of type-I and type-II, suggesting that CO_2 effervescence has occurred.

Siderite, associated with Pb–Zn sulfides, fills the interstices of euhedral quartz grains in stage-IV veins. Individual crystals of quartz are commonly cloudy owing to the presence of primary and secondary fluid inclusions and wispy, partly healed fractures. Because of the tiny size of its inclusions, siderite was excluded from

this study. Type-I and type-IV inclusions ranging in size from <5 to 20 μm were identified in quartz, and contain a vapor phase making up 10 to 20 vol.%.

Fluid-inclusion data

The fluid inclusions in skarn from the preore stage (stage I) are too small to use for microthermometric data. Table 5 summarizes the results of heating and freezing experiments for ore-forming fluids from later stages (II, III and IV) from the Ulsan deposit.

The massive skarns that formed during the early period of stage II consist mainly of fine-grained clinopyroxene and granular magnetite and calcite crystals cut by coarse-grained clinopyroxene and veinlets of anisotropic garnet. Primary inclusions of types I and III within iron-rich clinopyroxene from the late metasomatic portion of stage IIa show ranges of homogenization temperature, 370°–442°C and 379°–456°C, respectively (Fig. 8). Salinities of primary type-III inclusions in clinopyroxene range from 38.6 to 45.1 equiv. wt.% NaCl (Fig. 9). Unfortunately, type-I inclusions in clinopyroxene were found to be too small for accurate freezing experiments. Primary type-III inclusions in skarn calcite homogenize at temperatures from 361° to 464°C, with salinities of 32.9 to 38.2 equiv. wt.% NaCl. Secondary inclusions in calcite homogenize at temperatures of 222° to 347°C, with salinities of 31.3 to 36.8 equiv. wt.% NaCl. The presence of these hypersaline (up to 45 wt.% NaCl) and high-temperature (up to 460°C) fluids in stage II indicates that fluids responsible for prograde skarn may have had a magmatic source.

Primary inclusions in quartz are only of type III. They homogenize at temperatures from 251° to 340°C, with salinities of 30.1 to 35.2 equiv. wt.% NaCl. Primary inclusions in andradite in veins are only type-I inclusions and homogenize at temperatures from 404° to 452°C and have salinities of 16.9 to 24.5 equiv. wt.% NaCl. These less saline fluids indicate incursion of more
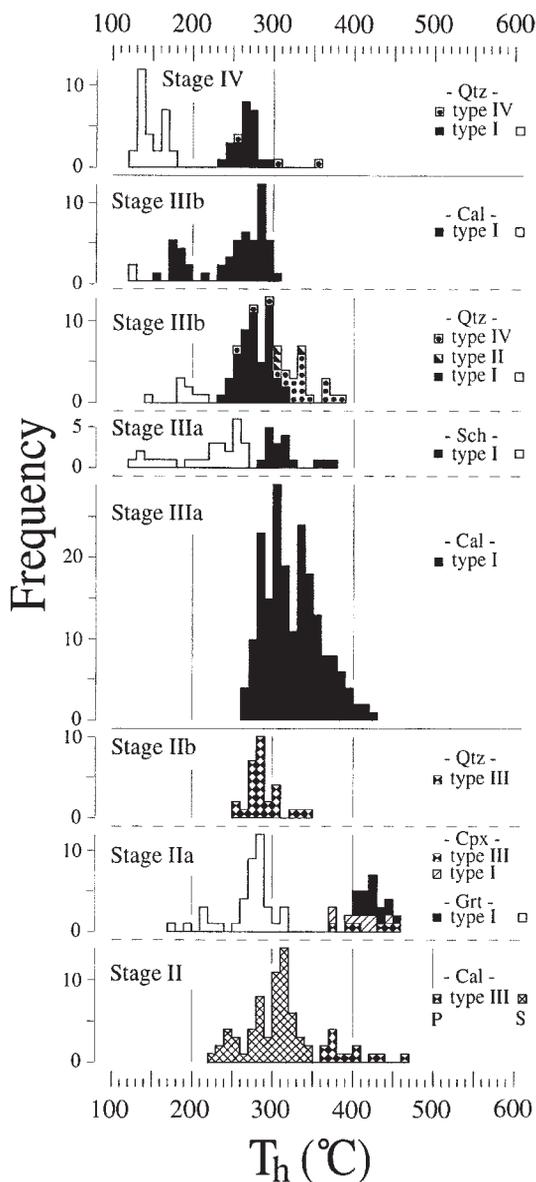

FIG. 8. Frequency histogram of total homogenization temperatures (T_h) for fluid inclusions in skarn and vein minerals from the Ulsan mine. For type-IV fluid inclusions, decrepitation temperatures before anticipated homogenization are used as minimum estimates of homogenization. Cal: calcite, Cpx: clinopyroxene, Grt: garnet, Qtz: quartz, and Sch: scheelite.

TABLE 5. SUMMARY OF FLUID-INCLUSION DATA FROM SKARN AND VEIN MINERALS IN STAGES II, III AND IV, ULSAN DEPOSIT, SOUTHEASTERN KOREA

Stage	Mineral	Type	Phase*	Homogenization temperature (°C) primary	secondary	Salinity (equiv. wt. % NaCl) primary	secondary
II	Calcite	III	L+V+Hl	361-464	222-347	32.9-38.2	31.3-36.8
IIa	Clinopyrox.	III	L+V+Hl	379-456	-	38.6-45.1	-
		I	L+V	370-442	-	-	-
	Garnet	I	L+V	404-452	170-315	16.9-24.5	9.5
IIb	Quartz	III	L+V+Hl	251-340	-	30.1-35.2	-
IIIa	Calcite	I	L+V	260-425	-	3.5-24.4	
IIIa	Scheelite	I	L+V	287-370	125-268	18.7-22.9	2.2-15.3
IIIb	Quartz	IV	L+CO₂	250-380	-	1.8-10.3	-
		II	V+L	300-334	-	8.0	-
		I	L+V	239-314	145-218	3.4-19.0	2.4-6.0
IIIb	Calcite	I	L+V	156-300	120	2.7-14.3	2.4-2.7
IV	Quartz	IV	L+CO₂	252-352	-	4.3-6.1	-
IV	Quartz	I	L+V	234-291	125-171	2.6-10.5	0.2-4.1

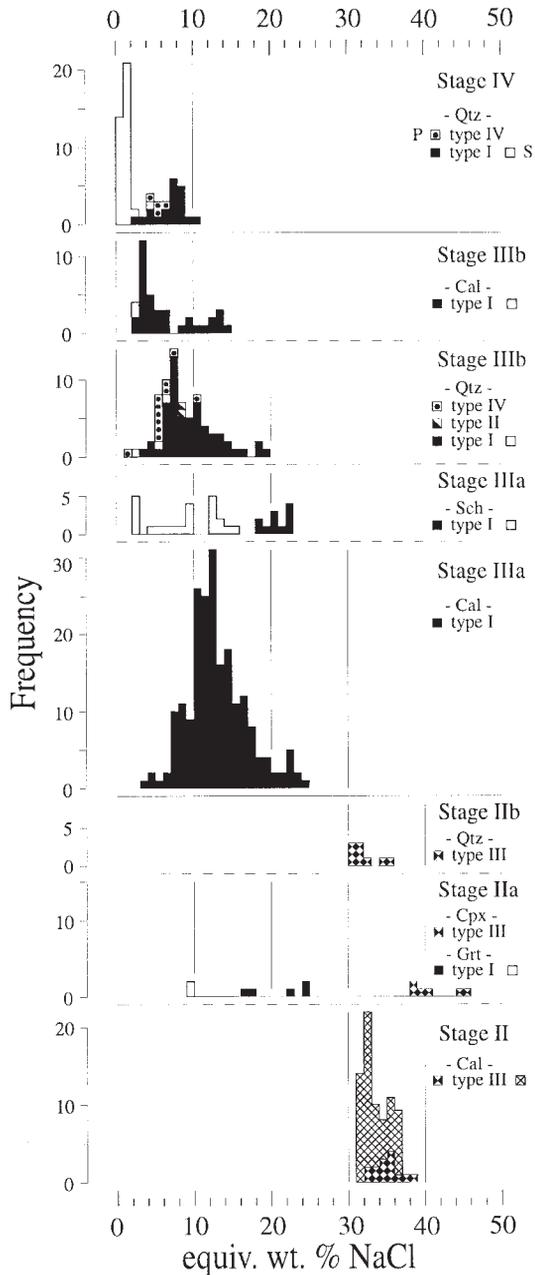*Abbreviations; Hl: halite, L: liquid, V: vapor.

FIG. 9.   Frequency histogram of salinity (equiv. wt.% NaCl)
for fluid inclusions in skarn and vein minerals of the Ulsan
mine. See Figure 8 for mineral abbreviations.

dilute near-surface fluids during the late metasomatic
portion of stage IIa. Secondary inclusions in garnet ho-
mogenize at a temperature between 170° and 315°C, and
have salinities near 9.5 equiv. wt.% NaCl.

Primary inclusions in calcite of stage III are all of
type I. They homogenize at temperatures from 260° to
425°C, with salinities of 3.5 to 24.4 equiv. wt.% NaCl.
Primary inclusions in scheelite also are of type I, and
homogenize from 287° to 370°C, with salinities of 18.7
to 22.9 equiv. wt.% NaCl. Secondary inclusions in
scheelite homogenize between 125° and 268°C, and
have salinities of 2.2 to 15.3 equiv. wt.% NaCl.

Primary inclusions in quartz include types I, II and
IV. The first melting of ice in type-I and type-IV inclu-
sions in quartz was recognized near –21°C, indicating
the predominance of NaCl among dissolved salts in later
periods of stage III. Type-I and type-II inclusions ho-
mogenize at temperatures from 239° to 314°C and from
300° to 334°C, respectively, with salinities of 3.4 to 19.0
and 8.0 equiv. wt.% NaCl, respectively. Temperatures
of final melting of solid CO_2 (T_m-CO_2) in primary type-
IV inclusions in quartz are –57.8° to –56.9°C. Homog-
enization of the CO_2-rich phase (T_h-CO_2) occurs at
temperatures of 12.2° to 27.9°C. Clathrate-melting tem-
peratures (T_m-clath, 4.2 to 9.1°C) correspond to salini-
ties between 1.8 and 10.3 equiv wt.% NaCl. Because
most type-IV inclusions decrepitated prior to total ho-
mogenization, only 17 estimates of temperatures of to-
tal homogenization (T_h-total) are available. They range
from 250° to 380°C. The similar ranges of temperature
in coexisting type-I and type-IV inclusions may indi-
cate CO_2 effervescence (fluid unmixing). Secondary
type-I inclusions in quartz homogenize from 145° to
218°C, and have salinities of 2.4 to 6.0 equiv. wt.%
NaCl.

Primary inclusions in calcite are only of type I and
homogenize between 156° and 300°C, with salinities of
2.7 to 14.3 equiv. wt.% NaCl. Secondary inclusions in
calcite homogenize near 120°C, and have salinities of
2.4 to 2.7 equiv. wt.% NaCl. These lower temperatures
of homogenization and salinities, compared to stage I,
likely indicate progressive mixing with near-surface flu-
ids.

Primary inclusions in quartz of stage IV are of type
I and type IV. Type-I inclusions homogenize from 234°
to 291°C, and have salinities of 2.6 to 10.5 equiv. wt.%
NaCl. Secondary type-I inclusions in stage-IV quartz
homogenize at temperatures of 125° to 171°C, and have
salinities of 0.2 to 4.1 equiv. wt.% NaCl. Though few
type-IV inclusions were measured, they are similar to
those in stage-III quartz, but have generally lower
T_h-total and higher T_m-clath values (T_h-total: 252° to
352°C; T_m-clath: 6.8° to 7.8°C).

Fluid-inclusion data from the Ulsan deposit indicate
that mineralization formed over wide ranges of tempera-
ture and salinity, which reflects multiple hydrothermal
episodes rather than one protracted event. Fluid inclu-
sions in stage II (prograde metasomatic event) consist
mainly of primary halite-bearing type-III inclusions,
whereas those of stage III (retrograde skarn) and stage
IV (vein) consist of types I, II, and IV, implying that
ore-forming fluids in the Ulsan deposit originated from

two distinct sources (Fig. 10). The decrease in salinity, from 45 to 2 equiv. wt.% NaCl, may correspond to drastic changes in the fluid-evolution history of the hydrothermal system, from dominantly magmatic to a mixture of magmatic and meteoric water. The distinct high-salinity trend in stage II could be the result of phase separation from a magma. There are no significant evaporite units known in the stratigraphic section in the Ulsan area. Thus the dissolution of evaporite units cannot be responsible for the high-salinity trend in the prograde-skarn stage. Also, there is no evidence of significant boiling in anhydrous skarn minerals in stage II. Thus boiling of a less saline fluid would be not expected. This highly saline fluid remained present over the entire range of temperature (250°–460°C) along the high-salinity trend. Thus release of a high-salinity fluid from an underlying body of magma is a realistic process to explain the high-salinity trend in the fluid-inclusion data. During stages III and IV, dilution of the highly saline fluid by mixing with less saline water could re-

sult in both low-salinity and low-temperature trends. There is evidence of sporadic boiling in the retrograde skarn and vein stages, suggesting that repeated fracturing must have occurred. The transition from conditions of lithostatic to near-hydrostatic pressure would allow meteoric fluids to interact with an initially magmatic hydrothermal system, resulting in the complexity of the fluid evolution within the Ulsan deposit.

DISCUSSIONS AND CONCLUSIONS

Pressure considerations

The maximum thickness of the sedimentary rock near the Gadae-Ri granite in the Ulsan mine area is approximately 2,500 m (Choi *et al.* 1980). This thickness is equivalent to a maximum lithostatic pressure at about 0.7 kbar. The Gadae-Ri granite pluton consists of equigranular hornblende–biotite granite in the center, but with porphyritic texture as well as miarolitic, gra-
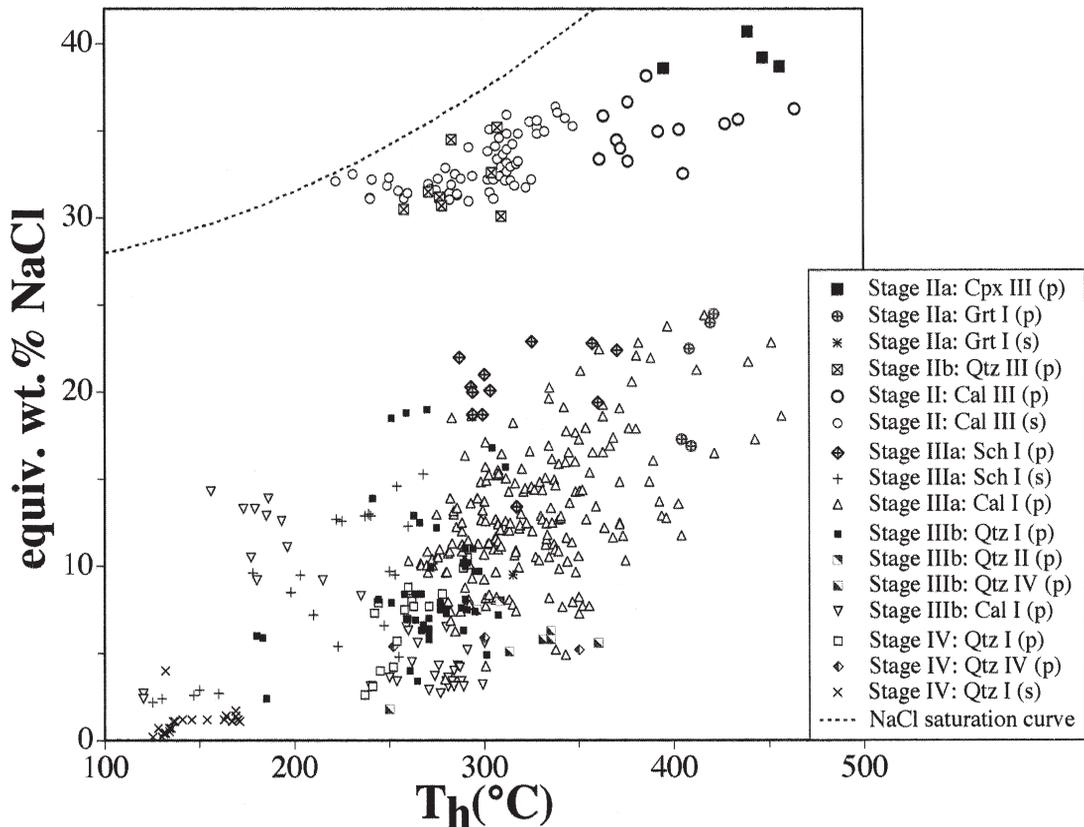

FIG. 10. Plot of homogenization temperature (T_h) *versus* salinity (equiv. wt.% NaCl) for fluid inclusions in minerals from various stages of mineralization. Stages I, II, III and IV following mineral names are types of fluid inclusions. See Figure 8 for mineral abbreviations; p: primary, s: secondary.

nophyric and micrographic textures toward the intrusive contact, indicative of high-level emplacement. Choi & Wee (1994) suggested that the magma in this pluton, with a minimum-melt bulk composition, crystallized at pressures of 0.5 to 2.0 kbar under H_2O-saturated conditions. The pluton is surrounded by a contact-metamorphic aureole in the sedimentary rocks, showing a steep geothermal gradient (Imai & Choi 1984). We suggest that the iron, tungsten and polymetallic mineralization is related to the intrusive activity of the Gadae-Ri granite pluton, probably at about 58–62.9 Ma.

Ore-forming conditions

Arsenopyrite, a common constituent of sulfide deposits, exhibits appreciable solid-solution dependence on temperature, sulfur fugacity and, to a lesser extent, pressure. Equilibrium compositions of arsenopyrite are usually preserved in hydrothermal deposits that have undergone relatively rapid cooling, and their compositions are not typically subject to change during subsequent processes. The arsenopyrite geothermometer was first proposed by Kretschmar & Scott (1976), and was re-examined by Sharp *et al.* (1985), but the geothermometer was not calibrated at temperatures below about 300°C. Scott (1983) also constructed a phase-equilibrium diagram in the Fe–Zn–As–S system in which the compositions of arsenopyrite and sphalerite are determined by temperature and sulfur fugacity. Thereafter, the arsenopyrite geothermometer has received considerable attention as a way of estimating the physicochemical conditions of those ore deposits that formed at temperatures higher than 300°C (Lowell & Gasparrini 1982, Kay & Strong 1983, Sundblad *et al.* 1984, Sharp *et al.* 1985, Bortnikov 1993).

In conjunction with arsenopyrite geothermometry and fluid-inclusion data (Tables 3, 5), an attempt was made to determine the physicochemical conditions of skarn formation and ore mineralization, and to propose a conceptual model for fluid evolution in the Ulsan hydrothermal system.

The distinctive high-salinity trend from the Ulsan deposit has been recognized in other porphyry-type deposits (Bodnar 1995). Yang (1996) found that primary type-III inclusions in vug and vein quartz within the Gadae-Ri granite homogenize at temperatures from 380° to 600°C, with salinities of 49 to 63 equiv. wt.% NaCl. This result indicates that the initial hypersaline hydrothermal fluid originated from the exsolution of magmatic fluids and metals from the upper levels of a porphyry intrusion, suggestive of mineralization in a porphyry-type magmatic–hydrothermal system (Corbett & Leach 1998). Initial penetration of hydrothermal fluids during the prograde-skarn stage led to the introduction of Si, Mg, Fe, Al, As and W, with concomitant leaching of Ca and expulsion of CO_2 from recrystallized limestone, resulting in deposition of anhydrous calcic skarn-forming minerals and magnetite. Skarn-forming

fluids in this stage are typically of high salinity (up to 45 equiv. wt.% NaCl) at a high temperature (up to 460°C) (Fig. 10). Ore-forming fluids trapped in fluid inclusions at this stage do not coexist with vapor-rich inclusions. A lack of cogenetic vapor-rich fluid inclusions indicates that high-salinity fluids (up to 45 equiv. wt.% NaCl) were generated by direct exsolution of an immiscible highly saline brine from a crystallizing granitic magma, and are not a product of aqueous fluid immiscibility (Cline & Bodnar 1994). Fluid flow was perhaps channeled primarily along fractures within recrystallized limestone, being driven by pressure gradients along a zone of higher permeability to initiate development of the pipe-shaped magnetite-dominant orebody. The rare occurrences of type-I inclusions in vein garnet and some late clinopyroxene, however, indicate that hypersaline fluids mixed locally with meteoric water within fractured massive skarn during the latter periods of stage IIa. During the late period of prograde skarn (stage IIb), fluids trapped in quartz also are hypersaline (30.1 to 35.2 equiv. wt.% NaCl) at temperatures of 251° to 340°C.

Following the deposition of magnetite in the main prograde skarn, the first deposition of arsenopyrite was associated mainly with stage-IIb prograde metasomatic skarn, intergrown with niccolite – rammelsbergite – gersdorffite – löllingite – native bismuth – bismuthinite – pyrrhotite. These common sulfides are characterized overall by a low sulfidation state during the main skarn stage. The nature of these arsenides and sulfarsenides can be considered to be a hybrid type, with a source transitional between magmatic ore fluid and material leached selectively from surrounding ultramafic rock. Such an origin would account for the deposition of the unusual Ni–Co-bearing minerals. Diagrams using the chemical compositions of arsenopyrite associated with these specific assemblages provide reliable estimations of temperature and $f(S_2)$ (Fig. 11). The Ni–Co-bearing nature of arsenopyrite A precludes its use as a geothermometer. The presence of löllingite + native bismuth ± pyrrhotite with the absence of bismuthinite constrain the stability field of arsenopyrite B. Arsenopyrite C coexists with native bismuth + bismuthinite and allows estimation of the temperature of Fe–As mineralization. The average compositions of arsenopyrite B and arsenopyrite C cluster at 34.39–35.37 atomic % As in the löllingite + native bismuth ± hexagonal pyrrhotite assemblage, and 33.85–34.14 atomic % As in the native bismuth ± bismuthinite assemblage, which corresponds to temperatures of 490° ± 25°C and 470° ± 10°C, respectively.

A slight decrease in ore-fluid temperature at the Ulsan mine also resulted in a change from löllingite- to arsenopyrite-saturated conditions. In this respect, it is noteworthy that the As-excess and S-deficient arsenopyrite in the stability field of löllingite indicates high temperatures (460° to 520°C). For the equilibrium assemblages arsenopyrite – löllingite – pyrrhotite and
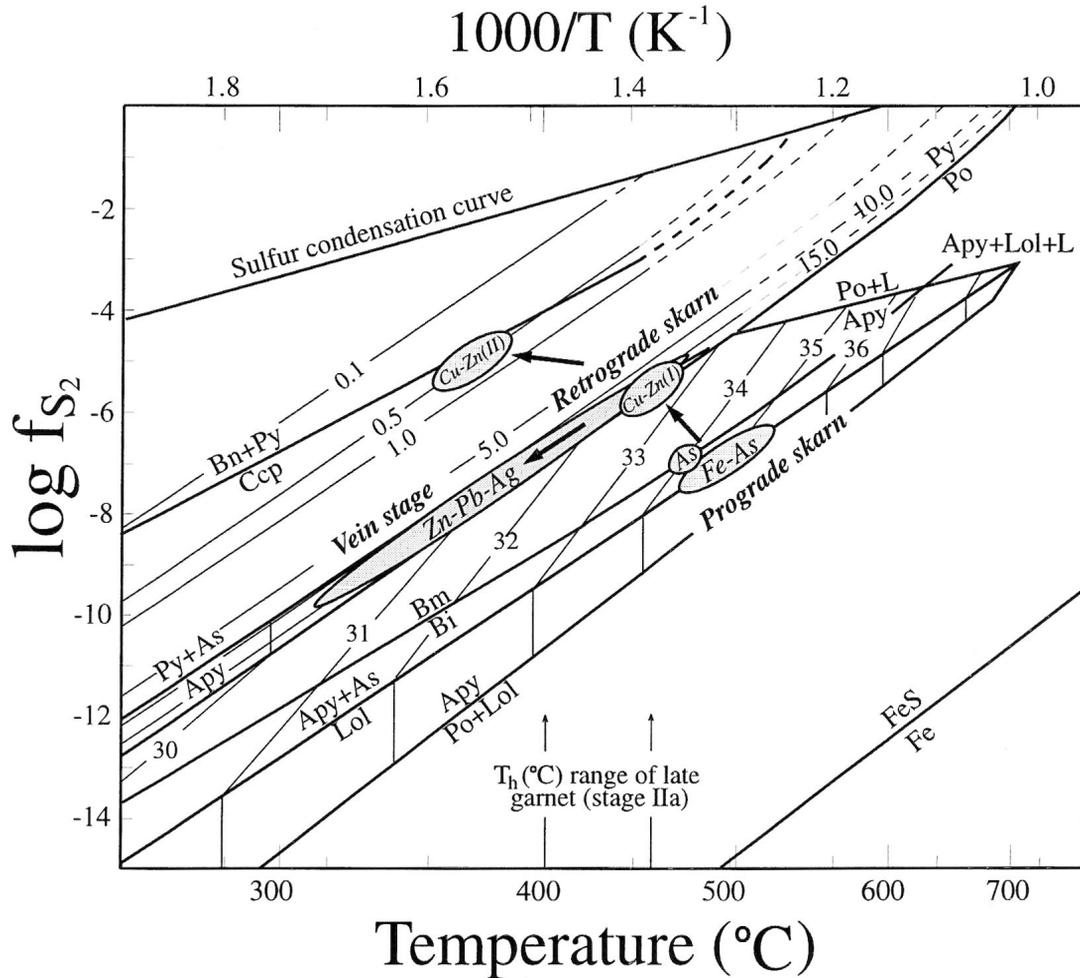
F IG. 11. Schematic model showing the compositional variation of arsenopyrite in sulfur fugacity and temperature and the evolution of ore fluids during different stages of mineralization at the Ulsan mine. Sulfur fugacity – temperature projection of the stability field of arsenopyrite given by Kretschmar & Scott (1976), and modified by Sharp *et al.* (1985), upon which the bismuth–bismuthinite buffer curve is superimposed. Arrows show an evolutionary trend from prograde skarn stage associated with Fe–As and As mineralization through retrograde skarn stage associated with Cu–Zn (I) and (II) mineralization to the vein stage associated with Zn–Pb–Ag mineralization. Apy: arsenopyrite, As: arsenic, Bi: bismuth, Bm: bismuthinite, Bn: bornite, Ccp: chalcopyrite, L: S–As liquid, Lol: löllingite, Po: pyrrhotite, and Py: pyrite.

arsenopyrite – native bimuth – bismuthinite, the sulfur fugacity can be determined from the arsenic content of arsenopyrite B and C, and is in the range $10^{-7.5}$ to $10^{-6.3}$ and $10^{-7.1}$ to $10^{-6.7}$ bars, respectively (Fig. 11).

Considering the inferred minimum pressure (0.5 kbar) equivalent to the stratigraphic depth, the temperatures of trapping of the fluid inclusions ($380° < T_h < 460°C$) in stage II can be pressure-corrected, based on the salinity of $NaCl–H_2O$ inclusions, 40 equiv. wt.% NaCl, and the data from Bodnar & Vityk (1994). The pressure-corrected temperatures in stage II range from 410° to

480°C. The temperatures ($470° \pm 30°C$) derived from the associations arsenopyrite – löllingite – native bismuth and arsenopyrite – native bismuth – bismuthinite are in fair agreement with the pressure-corrected temperature from late clinopyroxene and calcite crystallized during this stage II.

The ore-forming fluids in stage II show an evolutionary trend from high salinity and high temperature to high salinity and low temperature. This finding suggests that ore-forming fluids in the prograde-skarn stage underwent an overall simple cooling (Fig. 10).

During stage IIIa, retrograde skarn and W mineralization were formed from moderately saline liquids (3.5 to 24.4 equiv. wt.% NaCl) at temperatures of 260° to 425°C. Retrograde skarn may have formed owing to influx of meteoric water. However, amphibole, chlorite and quartz formed at a much lower temperature and salinity than clinopyroxene and garnet.

Moderate salinity (1.8 to 19.0 equiv. wt.% NaCl) fluids deposited hydrous silicates and Cu–Zn (I) mineralization in stage IIIb at temperatures of 156° to 380°C. The presence of arsenopyrite D (S-excess and As-deficient) buffered by hexagonal pyrrhotite and pyrite indicates relatively low temperatures compared to the stoichiometric composition FeAsS. On average, that arsenopyrite contains from 32.31 to 32.78 atomic % As, which corresponds to temperatures of 450° ± 20°C. Pressure-corrected fluid-inclusion temperatures are 380° ± 70°C and overlap the lower limit of temperatures indicated by the arsenopyrite geothermometer. The beginning of deposition of arsenopyrite D took place within a range of $f(S_2)$ near $10^{-6.0}$ to $10^{-5.2}$ bars. The later appearance of bornite, chalcopyrite, chalcocite, tennantite and then iron-poor sphalerite is characteristic of an overall high sulfidation state. The Cu–Zn ore marked "(II)" in Figure 11 implies a shift to higher $f(S_2)$ conditions. Cooling of the mineralizing fluids could have led locally to subsequent deposition of polymetallic sulfides under conditions that overlap the sulfidation curves of iron-poor sphalerite in the stability field of pyrite.

Low-salinity fluids (2.6 to 10.5 equiv. wt.% NaCl) led to Zn–Pb–Ag mineralization in stage IV at temperatures of 234° to 352°C. The difference of fluid compositions between stages III and IV may be due to influx of low-temperature – low-salinity fluids, presumably of meteoric origin. The average compositions of arsenopyrite E in association with pyrite exhibit a relatively wide variation, from 30.26 to 32.84 atomic % As. Temperature and sulfur fugacity estimated from these data are 310° to 470°C and $10^{-10.0}$ to $10^{-5.1}$ bars, respectively. Pressure-corrected fluid-inclusion temperatures are 320° ± 50°C, which overlap the lower temperatures indicated by the arsenopyrite geothermometer. Decreasing As contents of arsenopyrite, together with the appearance of pyrite, indicate a decrease in sulfur fugacity or temperature (or both) over this period.

Model of mineralization

On the basis of results of arsenopyrite geothermometry and the fluid-inclusion data, the evolutionary trend from hypersaline magmatic fluids associated with Fe mineralization to low-salinity, lower-temperature ore-forming fluids related to W–Cu–Zn and Zn–Pb–Ag mineralization suggests an influx of meteoric water into the waning hydrothermal system at deep levels along fractures. The relationship between homogenization temperature and salinity suggests a complex history of simple cooling, dilution and local CO_2 effervescence.

Decreasing As contents of arsenopyrite indicate a decrease in sulfur fugacity or temperature (or both) over all the stages of sulfide mineralization. Fe mineralization began above 464°C from a fluid containing greater than 45 equiv. wt.% NaCl. Considered to have a genetic relation to felsic magmatism, *i.e.*, the Gadae-Ri granite pluton, the nature of Fe–W and polymetallic mineralization at the Ulsan deposit may be regarded as having been formed at high temperatures and shallow depths (0.5 kbar). The formation of Ulsan skarn deposit may be due to its proximal position to a magma source, which is genetically related to a low-sufidation porphyry system.

REFERENCES

BODNAR, R.J. (1995): Fluid-inclusion evidence for a magmatic source for metals in porphyry copper deposits. *In* Magmas, Fluids, and Ore Deposits (J.F.H. Thompson, ed.). *Mineral. Assoc. Can., Short Course* **23**, 139-152.

_____ & VITYK, M.O. (1994): Interpretation of microthermometric data for H_2O–NaCl fluid inclusions. *In* Fluid Inclusions in Minerals: Methods and Applications (B. De Vivo & M.L. Frezzotti, eds.). Short Course of the IMA working group "Inclusions in Minerals" (Pontignano-Siena), 117-130.

BORTNIKOV, N.S. (1993): On the validity of arsenopyrite and arsenopyrite–sphalerite geothermometers. *Geol. Ore Deposits* **35**, 159-172.

BOZZO, A.T., CHEN, HSIAO-SHENG, KAAS, J.R. & BARDUHN, A.J. (1975): The properties of hydrates of chlorine and carbon dioxide. *Desalination* **16**, 303-320.

CHOI, H.I., OH, J.H., SHIN, S.C. & YANG, M.Y. (1980): Geology and geochemistry of the Gyungsang strata in Ulsan area. *Korea Res. Inst. Geosci. Mineral Resources* **20**, 1-33.

CHOI, S.G. & IMAI, N. (1985): Ni–Fe–Co arsenides and sulpharsenides from the Ulsan mine, Republic of Korea. *Mining Geol.* **35**, 1-16.

_____ & _____ (1993): Magnetite and scheelite-bearing skarns in Ulsan mine, Korea. *J. Kor. Inst. Mining Geol.* **26**, 41-54.

_____ & WEE, S.M. (1994): Petrochemical study of the Gadaeri granite in Ulsan area, Kyeongsang Province. *Econ. Environ. Geol.* **27**, 459-467.

CHOU, I-MING (1987): Phase relations in the system NaCl–KCl–H$_2$O. III. Solubilities of halite in vapor-saturated liquids above 445°C and redetermination of phase equilibrium properties in the system NaCl–H$_2$O to 1000° C and 1500 bars. *Geochim. Cosmochim. Acta* **51**, 1965-1975.

CLINE, J.S. & BODNAR, R.J. (1994): Direct evolution of brine from a crystallizing silicic melt at the Questa, New Mexico, molybdenum deposit. *Econ. Geol.* **89**, 1780-1802.

CORBETT, G.J. & LEACH, T.M. (1998): Gold–copper systems in porphyry environments. *In* Southwest Pacific Rim Gold–Copper Systems: Structure, Alteration and Mineralization (G.J. Corbett & T.M. Leach, eds.). *Econ. Geol., Spec. Publ.* **6**, 83-100.

CRAIG, J.R. & VAUGHAN, D.J. (1994): *Ore Microscopy and Ore Petrography* (2nd ed.). John Wiley & Sons, New York, N.Y.

DIAMOND, L.W. (1992): Stability of CO$_2$ clathrate hydrate + CO$_2$ liquid + CO$_2$ vapour + aqueous KCl–NaCl solutions: experimental determination and application to salinity estimations of fluid inclusions. *Geochim. Cosmochim. Acta* **56**, 273-280.

HAYNES, F.M. (1985): Determination of fluid inclusion compositions by sequential freezing. *Econ. Geol.* **80**, 1436-1439.

IMAI, N. & CHOI, S.G. (1984): The first Korean occurrence of roquesite. *Mineral. J.* **12**, 162-172.

JIN, M.S., KIM, S.Y. & LEE, J.S. (1981): Granitic magmatism and associated mineralization in the Gyeongsang basin, Korea. *Mining Geol.* **31**, 245-260.

KAY, A. & STRONG, D.F. (1983): Geologic and fluid controls on As–Sb–Au mineralization in the Moretons Harbour area, Newfoundland. *Econ. Geol.* **78**, 1590-1604.

KRETSCHMAR, V. & SCOTT, S.D. (1976): Phase relations involving arsenopyrite in the system Fe–As–S and their application. *Can. Mineral.* **14**, 364-386.

LEE, S.M., KIM, S.W. & JIN, M.S. (1987): Igneous activities of the Cretaceous to the early Tertiary and their tectonic implications in South Korea. *J. Geol. Soc. Korea* **23**, 338-359.

LEE, Y.J. & UEDA, Y. (1977): K–Ar dating on granitic rocks from the Eonyang and Ulsan areas, Korea. *J. Mineral. Petrol. Econ. Geol.* **72**, 367-372.

LOWELL, G.R. & GASPARRINI, C. (1982): Composition of arsenopyrites from topaz greisen veins in southeastern Missouri. *Mineral. Deposita* **17**, 229-238.

PARK, H.I., CHOI, S.W., CHANG, H.W. & CHAE, D.H. (1985): Copper mineralization at Haman–Gunbuk mining district, Kyeongnam area. *J. Korean Inst. Mining Geol.* **18**, 107-124.

POTTER, R.W., III, CLYNNE, M.A. & BROWN, K.L. (1978): Freezing point depression of aqueous sodium chloride solutions. *Econ. Geol.* **73**, 284-285.

REEDMAN, A.J., PARK, K.H. & EVANS, J.A. (1989): The age of granitoid intrusions and related mineralisation in the Chisulryoung mountain area, southeast Korea: constraints on the age of the Chisulryoung volcanic formation and Yucheon group volcanism. *J. Geol. Soc. Korea* **25**, 51-58.

ROEDDER, E. (1984): The origin of inclusions. *In* Fluid Inclusions (E. Roedder, ed.). *Rev. Mineral.* **12**, 11-45.

SCOTT, S.D. (1983): Chemical behaviour of sphalerite and arsenopyrite in hydrothermal and metamorphic environments. *Mineral. Mag.* **47**, 427-435.

SHARP, Z.D., ESSENE, E.J. & KELLY, W.C. (1985): A re-examination of the arsenopyrite geothermometer: pressure considerations and applications to natural assemblages. *Can. Mineral.* **23**, 517-534.

STERNER, S.M., HALL, D.L. & BODNAR, R.J. (1988): Synthetic fluid inclusions. V. Solubility relations in the system NaCl–KCl–H$_2$O under vapor-saturated conditions. *Geochim. Cosmochim. Acta* **52**, 989-1005.

SUNDBLAD, K., ZACHRISSOU, E., SMEDS, S.A., BERGLUND, S. & ÅLINDER, C. (1984): Sphalerite geobarometry and arsenopyrite geothermometry applied to metamorphosed sulfide ore in Swedish Caledonides. *Econ. Geol.* **79**, 1660-1668.

WOO, Y.K., LEE, M.S. & PARK, H.I. (1982): Studies on the skarn-type ore deposits and skarn minerals in Gyeongnam Province. *J. Korean Inst. Mining Geol.* **15**, 1-16.

WOODS, T.L., BETHKE, P.M., BODNAR, R.J. & WERRE, R.W. (1981): Supplementary components and operation of the U.S. Geological Survey gas-flow heating/freezing stage. *U.S. Geol. Surv., Open-File Rep.* **81-954**, 1-12.

YANG, K.H. (1996): Fluid inclusions trapped in quartz veins and granitic rocks from Pusan–Kyeongju area. *J. Geol. Soc. Korea* **32**, 431-446.